Simulations of Infrared Spectra of Nanoconfined Liquids: Acetonitrile Confined in Nanoscale, Hydrophilic Silica Pores[†]

Christine M. Morales[‡] and Ward H. Thompson*

Department of Chemistry, University of Kansas, Lawrence, Kansas 66045

Received: August 14, 2008; Revised Manuscript Received: September 30, 2008

The infrared spectrum of acetonitrile confined in hydrophilic silica pores roughly cylindrical and 2.4 nm in diameter has been simulated using molecular dynamics. Hydrogen bonding interactions between acetonitrile and silanol groups on the pore wall involve charge transfer effects that have been incorporated through corrections based on electronic structure calculations on a dimer. The simulated spectrum of confined acetonitrile differs most prominently from that of the bulk liquid by the appearance of a blue-shifted shoulder, in agreement with previous experimental measurements. The dominant peak is little changed in position relative to the bulk liquid case, but broadened by ∼40%. A detailed analysis of the structure and dynamics of the confined liquid acetonitrile is presented, and the spectral features are examined in this context. It is found that packing effects, hydrogen bonding, and electrostatic interactions all play important roles. Finally, the molecular-level information that can be obtained about the dynamics of the confined liquid from the infrared line shape is discussed.

1. Introduction

Chemical reactivity in nanostructured materials, both naturally occurring and synthetic, is an issue of immense importance and current interest. For example, microporous and mesoporous metal oxides such as silica are used industrially for a variety of chemical transformations and are being explored as scaffolds for catalysis.[1,2] Fundamental to the success of chemical reactivity in such porous materials is the structure and dynamics of liquids when confined to pores with diameters of a few to tens of nanometers.

A number of recent studies have begun to uncover the unique properties of nanoconfined liquids. In particular, infrared and Raman spectroscopies have been used to probe both liquid structure and dynamics. The Jonas,[3,4] Fourkas,[5] Fayer,[6−8] Owrutsky,[9−11] Schmuttenmaer,[12] Zerda,[13] and other[14−18] research groups have shown experimentally that confinement can lead to peak shifts and modification of vibrational line shapes. Such data have been analyzed for widely different confining frameworks in shape, size, and chemical functionality and have been interpreted in the context of a number of models for the nanoconfined liquid structure and dynamics. On the other hand, molecular simulations[19−22] provide detailed models of confined liquid structure and dynamics and the resulting vibrational spectra. Such simulations can be valuable because they may facilitate interpretation of the existing data and prompt new experimental investigations. Ultimately, a deeper mechanistic understanding of how liquids move and interact within a nanoconfined structure may inspire the design of new technologies that exploit the unique physical properties of liquids in these confined environments.

A particular focus within our group has been the study of liquids within porous silica materials.[23−25] These are models of sol−gels, which can be synthesized with fairly regular pore diameters on the order of nanometers, making them ideal for controlled studies with pore size as an independent variable. In addition, their surface chemistry can be modified; for example, hydrophilic pores with surface silanol groups can easily be converted to hydrophobic pores with surface silyl esters by boiling in a terminal alcohol such as *tert*-butyl alcohol.[26] As is discussed below in section 2.1, the present study builds upon an atomistic molecular model that was developed in our group to study liquids in silica pores with varying sizes and surface chemistry.[23−25] Finally, we note that silica gels are sufficiently transparent to permit the study of their contents by infrared and Raman spectroscopies.

Vibrational spectroscopies are frequently used to probe both liquid structure and dynamics in confinement. Vibrational line shifts, dephasing times, population relaxation times, and reorientation times are among the properties that have been found to change with the size of nanoscale confining frameworks such as silica glasses[3−5,13−17] or reverse micelles.[6−12,18] However, the interpretation of these experimental data often relies on physical models with molecular-level implications that are difficult to test.

For example, a two-state, or core−shell, model is widely applied to explain the dependence of observable properties on pore size. Such a model assumes that all liquid properties are identical to bulk properties in the pore interior but are different for a layer of molecules near the surface of the confining framework. In particular, vibrational spectra are modeled as the average of spectral contributions from "surface" and "bulk" populations. For water in reverse micelles, Fayer and co-workers have explained the vibrational spectra and population relaxation times using the core−shell model, although rotational and vibrational correlation functions did not fit the core−shell model.[6−8] Similarly, infrared line shapes for the O−H libration in water and methanol in reverse micelles have been explained using a two-state model.[12] A core−shell explanation for confinement effects on these line shapes is supported by recent computer simulations by Schmuttenmaer and co-workers.[19] In porous silica, a two-state model has been applied to vibrational

---

[†] Part of the "Max Wolfsberg Festschrift".

* Corresponding author, wthompson@ku.edu.

[‡] Current address: Department of Chemistry, Iona College, 715 North Ave., New Rochelle, NY 10801.

10.1021/jp8072969 CCC: $40.75

properties such as dephasing of the C−D stretch of $CDCl_3$[5] and the S−O stretching band of DMSO,[3] based on a reasonable fit to the data versus pore radius over the available range of pore sizes.

Although the two-state model of confined liquids often fits macroscopic data such as the vibrational peak position and line shape, these fits to a limited data set cannot rule out other physical explanations that reproduce the data. For example, the conformational equilibrium of ethylene glycol[27] can be fit by a two-state model, but this interpretation has recently been called into question in light of computer simulations by our group.[24] Further, because computer simulations provide direct evidence of a microscopic basis for observed properties, they can also provide insight into the nature of molecular motions and intermolecular interactions responsible for changes in the spectra.

In the present work, we present the results of molecular simulations of the structure and infrared spectra of confined CH_3CN in nanoscale silica pores. The infrared spectrum of bulk CH_3CN is well-known[28] and understood. The ν_2 stretch of CH_3CN is particularly sensitive to its environment and is capable of accepting a hydrogen bond from a hydroxyl group.[29−33] Isotropic Raman spectra are available for the ν_1 (symmetric C−H) and ν_2 (C≡N) stretches of CH_3CN in the bulk and in silica pores with diameters of 24 and 33 Å.[13] In the published spectra, a shoulder appears upon confinement in 33 Å pores and grows larger upon confinement in 24 Å pores. The full width at half-maximum (fwhm) of the primary ν_2 peak in the Raman spectrum is about 40% wider when CH_3CN is confined to the 24 Å pores. The infrared spectrum has also been measured for the ν_2 stretch of CH_3CN in the bulk and in MCM-41 silica pores with diameters of 20, 29, and 36 Å.[34] In the infrared spectra of confined CH_3CN in MCM-41, the ν_2 peak and shoulder are of comparable intensity for 20 Å pores, in contrast to the Raman spectrum of confined CH_3CN in 24 Å sol−gel pores, in which the shoulder intensity is much smaller than that of the main peak. In both cases, the shoulder peak grows in relative intensity as the pore size is decreased.

Fourkas and co-workers have used optical Kerr effect (OKE) experiments to study the orientational dynamics of CH_3CN confined to silica gels with pores 24 and 44 Å in diameter.[35−37] In contrast to a single-exponential OKE decay for bulk CH_3CN, the decay of the OKE signal for confined CH_3CN is best described by a linear combination of three exponentials, the fastest of which is similar to the decay time for the bulk liquid. The slowest decay, on the order of tens of picoseconds, was interpreted by Fourkas and co-workers as coming from CH_3CN reorientation in the surface layer, while the intermediate time scale was attributed to CH_3CN exchange between the surface layer and the pore interior. Further, an explicit structural model was proposed in which some of the CH_3CN molecules near the surface are strongly hydrogen bonded to surface silanol groups, while the remaining CH_3CN molecules are interdigitated among those and are capable of exchanging into the pore interior. The structure and rotational dynamics probed by such experiments are naturally important in determining the IR spectra (vide infra).

Also at issue are the physical models used to describe the liquid structure of confined CH_3CN and potentially slower vibrational dynamics in confinement. For example, the model recently proposed by Fourkas and co-workers[37] includes a substantial (≈40%) population of strongly bound surface species within a persistent, solid-like antiparallel structure that should have very different vibrational dynamics than bulk CH_3CN. On the other hand, dephasing times very similar to bulk CH_3CN have been reported[13] on the basis of standard vibrational line shape analysis using equations due to Kubo.[38] The present work seeks insight on a molecular level to explain how the structure and dynamics of confined CH_3CN give rise to the observed vibrational line shapes.

One advantage of explicit molecular simulations is their direct and quantitative information about the physical structure of a liquid. It is well-known[20,21,39,40] that liquids have a tendency to organize themselves in layers radiating inward from the wall of a confining framework. A consequence of this organized structure is that the orientational preferences of molecules can vary from layer to layer. While the main focus of this work is to model vibrational properties, the liquid structure and orientational dynamics affect the vibrational line shape. In the present work therefore, we explore the distributions of molecular positions and orientations as well as the distribution of C≡N vibrational frequencies as a function of the molecule−wall distance. A central question is how the structure of CH_3CN confined to porous silica relates to the distribution of C≡N stretching frequencies. How do CH_3CN−surface interactions such as hydrogen bonding affect the vibrational frequencies of molecules near the pore walls? Are the effects of confinement limited to molecules near the surface, or are the vibrational frequencies also affected by changes in liquid structure throughout the pore? Ultimately, how does the overall distribution of frequencies in a pore differ from that of bulk CH_3CN?

While, as noted above, confinement to 24 Å silica pores is known to have a dramatic effect on orientational dynamics probed by optical Kerr effect spectroscopy,[35−37] line shape analysis of the one-dimensional infrared spectra suggests that CH_3CN reorientation times are not significantly modified upon confinement.[41] Thus, a number of questions remain regarding the molecular-level origin of spectral features. Are the vibrational dynamics of CH_3CN substantially slowed in confinement? Can time scales for vibrational dephasing be associated with movement of CH_3CN within a surface layer or with exchange from a surface layer into the pore interior? How do orientational and vibrational correlation times for confined CH_3CN relate to observed dephasing times extracted from vibrational line shapes using a standard Kubo analysis? To answer these questions, vibrational and orientational correlation functions are explicitly calculated within the model and are used to simulate the infrared line shape.

The remainder of the paper is organized as follows. The approach to calculating the infrared spectra and associated structural and dynamical properties of bulk and confined acetonitrile is outlined in section 2. In particular, a method for accounting for the hydrogen bonding-induced blue shift in the CN stretch, due to charge transfer interactions, is described. The calculated spectra for bulk and confined acetonitrile are presented in section 3, where the effects of the charge transfer hydrogen bonding and pore heterogeneity are also probed. The origins of the observed spectral features are examined in section 4 which necessarily involves a discussion of the structure and dynamics of confined acetonitrile compared to the bulk liquid. Finally, some conclusions are offered in section 5 along with directions for future investigations.

2. Methods

2.1. Model for CH_3CN in Silica Pores. A model for surface-modified silica pores recently has been developed to facilitate the study of confined liquids in these pores.[23−25] An advantage of this model is the use of a number of distinct pore structures to reflect pore heterogeneity in real systems.[23] This heterogeneity

TABLE 1: Potential Parameters[a]

atom type	σ (Å)	ϵ (eV)	q (e)	m (amu)	ref
CH_3	3.480	0.01384630	0.2870	15.035	43
C	3.287	0.00362740	0.1376	12.011	43
N	3.190	0.00362740	−0.4246	14.007	43
Si	2.500	0.00000434	1.2800	28.000	24
O^b	2.700	0.01981744	−0.6400	16.000	24
O^{nb}	3.070	0.00737191	−0.7400	16.000	24
H	1.295	0.00001586	0.4200	1.000	24

[a] $r(C-CH_3) = 1.46$ Å, $r(C-N) = 1.17$ Å from ref 43.

can have a profound effect on some properties of confined liquids, particularly those that are strongly affected by specific interactions with the pore surface.[24] Most recently, grand canonical Monte Carlo simulations have been used to determine the equilibrium density of liquid in the pores.[25] The present work builds on these previous studies by using the predetermined equilibrium density of CH_3CN in silica pores within our model. The liquid density is believed to be an important detail because the experimental Raman spectra of CH_3CN in sol−gel pores[13] and the IR spectra in MCM-41 pores[34] have been shown to vary at lower liquid densities.

2.2. Simulation Details. Classical molecular dynamics calculations were carried out using DL_POLY_2 software[42] with minor modifications to evaluate vibrational frequencies. Periodic boundary conditions were applied for bulk and confined simulations. Bulk simulations consisted of a cubic box, 28.3736 Å on a side, containing 256 CH_3CN molecules for a density of 0.764 g/cm^3. To simulate confined CH_3CN, each silica pore was simulated within a rectangular periodic box with the following dimensions: 30 Å long in the direction of the pore axis and 44 Å on a side along the remaining two axes. The interior diameter of each pore studied was ≈24 Å.

The rigid, three-site ANL model for acetonitrile[43] was used without modification. The associated Lennard-Jones parameters and charges are listed in Table 1 along with our parameters for surface-hydroxylated silica pores. Si and bridging O atoms were frozen throughout our simulations. Surface hydroxyl groups were allowed to move with the following constraints: (1) Si−O^{nb} distances were frozen to 0.950177 Å, (2) O^{nb}−H distances were harmonically constrained to 1.663 Å with a force constant of 85.056 eV/Å, and (3) Si−O^{nb}−H angles were harmonically constrained to 118.5° with a force constant of 2.1248 eV/rad^2.

Lennard-Jones interactions were evaluated with a cutoff of 15 Å. The smoothed particle mesh Ewald summation was used to evaluate electrostatic interactions with an Ewald parameter of $\alpha = 0.25$, $10 \times 10 \times 8$ k-point grid for fast Fourier transforms, and a cutoff of 15 Å.

Simulations of bulk CH_3CN were initiated from a face-centered cubic lattice and begun with a 1 ns equilibration phase with 2 fs time steps, during which velocity rescaling was used to achieve a simulation temperature of approximately 300 K. Data were then collected over a 1 ns trajectory with 1 fs time steps in the NVE ensemble. Simulations of CH_3CN in each of 10 model silica pores were initiated from configurations obtained from prior equilibration by grand canonical Monte Carlo[25] and were equilibrated for 500 ps with 2 fs time steps during which a Nosé-Hoover thermostat with a time constant of 1 ps was used to achieve a simulation temperature of approximately 300 K. Data were then collected over trajectories in the NVT ensemble, using the same thermostat and temperature, for 1 ns with 2 fs time steps.

Additional simulations were carried out in each of the 10 model pores with two modified potentials: (1) with no charge on the H atom of the hydroxyl group and (2) with no charges on any of the Si, O, and H atoms of silica. As will be discussed in detail, the two modifications were used to compare the specific effects of hydrogen bonding interactions to those of overall electrostatic interactions with the pore.

2.3. Model for Vibrational Frequencies and Line Shapes. To model the effects of confinement on the ν_2 stretch in the infrared spectrum of CH_3CN, we have used two layers of theory. First, a perturbation theory expression is used to obtain vibrational frequencies from the classical molecular dynamics trajectories. Second, an electronic structure based correction term is applied to approximately address quantum effects on the ν_2 vibration in hydrogen-bonded CH_3CN molecules. Ideally, quantum effects on intermolecular forces due to hydrogen bonding should be allowed to influence the trajectory as well as the instantaneous vibrational frequencies. A full quantum molecular dynamics simulation would be unfeasible given the time scales required, however.

A first-order perturbation theory expansion[44] was used to obtain the frequency $\omega(t)$ along the oscillator coordinate Q, in terms of the classical forces $\partial V(t)/\partial Q$ from the molecular dynamics trajectory

$$\hbar\omega(t) = (\langle\psi_1|Q|\psi_1\rangle - \langle\psi_0|Q|\psi_0\rangle)\,\frac{\partial V(t)}{\partial Q} + ... \tag{1}$$

where ψ_0 and ψ_1 are the ground- and first excited-state vibrational eigenfunctions for the isolated molecule. We note that this first-order expansion neglects higher-order derivatives as well as interactions between the ν_2 stretch and other vibrational normal modes. Further, we use a fully localized C≡N stretch as a model of the ν_2 vibrational normal mode. The force along the bond is therefore obtained as follows:[45,46]

$$\frac{\partial V}{\partial Q} = \sum_i \frac{\partial V}{\partial \xi_i}\frac{\partial \xi_i}{\partial Q} \tag{2}$$

$$= -\sum_i F_i \frac{\partial \xi_i}{\partial Q} \tag{3}$$

$$= \left[\frac{\mu}{m_C}\vec{F}_C - \frac{\mu}{m_N}\vec{F}_N\right]\hat{r}_{CN} \tag{4}$$

The quantum matrix elements $Q_{nn} = \langle\psi_n|Q|\psi_n\rangle$ are obtained for a single oscillator with cubic anharmonicity (eq 5) to model the unperturbed ν_2 stretch of CH_3CN. The potential form of the oscillator is as follows

$$U(Q) = (\mu\omega_0^{\,2}/2)Q^2 + (f/6)Q^3 \tag{5}$$

It can be shown[47] that for an oscillator with a given cubic anharmonicity constant[48] $f = 5.566 \times 10^{30}$ cm^{-4} and unperturbed frequency[32] $\omega_0 = 2266$ cm^{-1}, the required matrix elements are easily obtained

$$Q_{11} - Q_{00} = -\frac{f}{2\hbar\omega_0}\left(\frac{\hbar}{\mu\omega_0}\right)^2 \tag{6}$$

Because hydrogen bonding within the simple classical model is modeled as a purely electrostatic attraction, naïve application of the first-order perturbation theory expression would lead to a red shift in the ν_2 vibrational frequency for hydrogen bonded CH_3CN molecules. Hydrogen bonding is known to give rise to a blue shift in the ν_2 vibrational frequency that can only be reproduced by including quantum effects on the frequency shift. In line with previous theoretical work,[49] our calculations confirm that this blue shift is associated with shortening and strengthening of the C≡N bond due to charge transfer from the lone pair

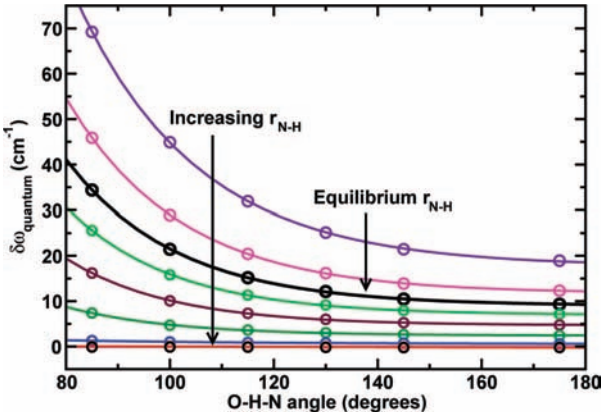

Figure 1. Vibrational frequency shifts in cm^{-1} from quantum calculations, as a function of O−H−N angle and N−H distance. Calculated frequency shifts are shown for angles between 85° and 175° and for N−H distances between 1.86 and 6.11 Å. See text for a discussion of the calculation methodology.

on the N atom to the O−H antibond. The quantum calculations and associated corrections are explained below in detail.

The infrared line shape is described[38,50] as a Fourier transform of the semiclassical correlation function $\phi(t)$

$$I(\Delta\omega) = \frac{1}{2\pi}\int_{-\infty}^{\infty} \mathrm{d}t\, \mathrm{e}^{-i\Delta\omega t}\phi(t) \tag{7}$$

The correlation function $\phi(t)$ can be written

$$\phi(t) = \mathrm{e}^{-|t|/T_1}\langle \hat{\underline{\mu}}(0) \cdot \hat{\underline{\mu}}(t)\mathrm{e}^{i\int_0^t \delta\omega(\tau)\mathrm{d}\tau}\rangle \tag{8}$$

where T_1 is the population relaxation time scale, where $\delta\omega(t) \equiv (\omega(t) - \langle\omega\rangle)$, and $\hat{\mu}$ is the $0 \rightarrow 1$ (fundamental) transition dipole vector for the CN oscillator. Because hydrogen bonding can have a significant effect on transition dipoles,[51] changes in the transition dipole due to hydrogen bonding were modeled by an analytical fit to transition dipoles from quantum calculations as described below in more detail. A literature value[52] of $T_1 = 80$ ps for the ν_2 vibration is substantially longer than the time scale for the decay of ϕ, so we have neglected population relaxation in calculating $\phi(t)$.

In probing the vibrational dynamics, it is also interesting to examine the normalized frequency autocorrelation function $C_\omega(t)$, defined by

$$C_\omega(t) \equiv \langle\delta\omega(0)\delta\omega(t)\rangle/\langle\delta\omega^2\rangle \tag{9}$$

The frequency autocorrelation function, a fundamental dynamical quantity for condensed phase liquids, can provide a time scale, τ_ω, for pure vibrational dephasing[38,53]

$$\tau_\omega \equiv \int_0^\infty C_\omega(t)\,\mathrm{d}t \tag{10}$$

This time scale can in turn be related to microscopic changes in intermolecular forces.

2.4. Quantum Effects of Hydrogen Bonding on Frequencies and Transition Dipoles. The origin of the ν_2 blue shift upon hydrogen bonding was explored through quantum calculations using the O3LYP[54] hybrid functional and the 6-311++G-(3df,3pd) Pople-style triple-ζ basis set with polarization and diffuse functions[55−57] within the Gaussian 03 software package.[58] A complex between one CH_3CN molecule and one SiH_3OH molecule was optimized in vacuo as a simple model for the hydrogen bonds formed at the interface. Natural bond orbital[59] calculations on the optimized complex show charge transfer from the N lone pair on CH_3CN to the O−H antibond on SiH_3OH; such charge transfer can strengthen the C≡N bond by removing electron density from an orbital that has antibonding character. Calculated geometries at this level of theory are also consistent with a stronger C≡N bond: the C−N distance is 1.67 Å for a free CH_3CN molecule but only 1.65 Å for the complex. The blue shift in the stretching frequency can thus be attributed to a shorter and stronger C≡N bond upon formation of a hydrogen bond.

To obtain quantum corrections for hydrogen bonded CH_3CN, the transition dipole and fundamental vibrational transition energy were calculated quantum mechanically as a function of the N−H distance and the O−H−N angle. This was accomplished by solving the vibrational Schrödinger equation approximately for the lowest three vibrational eigenstates. A (0 to ∞) sinc-function discrete variable representation (DVR) basis[60,61] was used, in which the kinetic energy matrix can be obtained analytically and the potential energy matrix is assumed to be diagonal.[62,63] An evenly spaced grid was used, consisting of 40 DVR grid points over a 0.4 Å range centered at the equilibrium bond distance. Potential energies used to construct the Hamiltonian, as well as the total dipole moment, were evaluated at each grid point using Gaussian 03 single point calculations. Transition dipoles were evaluated directly using ground and excited-state wave functions in the DVR basis. Quantum vibrational frequency shifts are shown in Figure 1 as a function of the N−H distance and the O−H−N angle, two geometrical parameters associated with hydrogen bonding. These were compared with the corresponding frequency shifts evaluated with the same DVR basis but using the classical potential, to obtain the difference between quantum and classical descriptions of the ν_2 vibrational frequency shift. At each N−H distance, this difference was fit to a single exponential decay, plus a constant shift as a function of the O−H−N angle θ

$$\nu_{\text{quantum}} - \nu_{\text{classical}} = A\mathrm{e}^{-\alpha(\theta-\theta_0)} + B \tag{11}$$

where $\theta_0 = 70°$. The three fit parameters, A, α, and B, vary smoothly as a function of the N−H distance. These three parameters were each fit to an analytical function:

$$A = a_A\mathrm{e}^{-\eta_A(r-r_0)} + b_A\mathrm{e}^{-\xi_A(r-r_0)} \tag{12}$$

$$\alpha = a_\alpha\mathrm{e}^{-\eta_\alpha(r-r_0)} + \frac{b_\alpha}{1 + \mathrm{e}^{\xi_\alpha(r-r_0-\Delta)}} \tag{13}$$

$$B = a_B\mathrm{e}^{-\eta_B(r-r_0)} + b_B\mathrm{e}^{-\xi_B(r-r_0)} \tag{14}$$

with $r_0 = 2.10927$ Å. The resulting analytical expression was used as a correction term and added to the vibrational frequencies obtained from perturbation theory for all CH_3CN molecules. Though approximate, this quantum correction captures major effects of hydrogen bonding on the infrared line shape such as the prominent shoulder on the high-frequency side of the ν_2 peak and is therefore believed to be sufficient for the present mechanistic analyses. A similar analysis was used to construct an analytical expression for the transition dipole moment

$$\langle\psi_0|\mu|\psi_1\rangle = C\mathrm{e}^{-\beta\theta} + D \tag{15}$$

$$C = a_C\mathrm{e}^{-\eta_C(r-r_0)} \tag{16}$$

$$\beta = a_\beta\mathrm{e}^{-\eta_\beta(r-r_0)} \tag{17}$$

$$D = a_D\mathrm{e}^{-\eta_D(r-r_0)} \tag{18}$$

The fit parameters are given in Table 2. A more accurate treatment incorporating quantum effects on the molecular

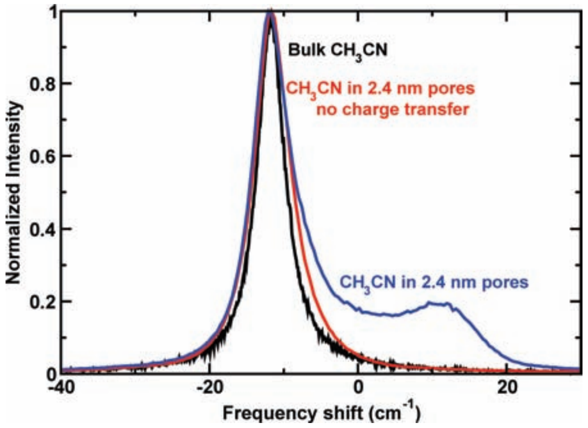

Figure 2. Simulated infrared spectrum for the C$\equiv$N stretch of CH$_3$CN in the bulk liquid and confined to $\approx$2.4 nm diameter silica pores. Line shapes for bulk CH$_3$CN (black line), confined CH$_3$CN averaged over 10 pores (blue line), and confined CH$_3$CN without the charge transfer hydrogen-bonding correction (red line).

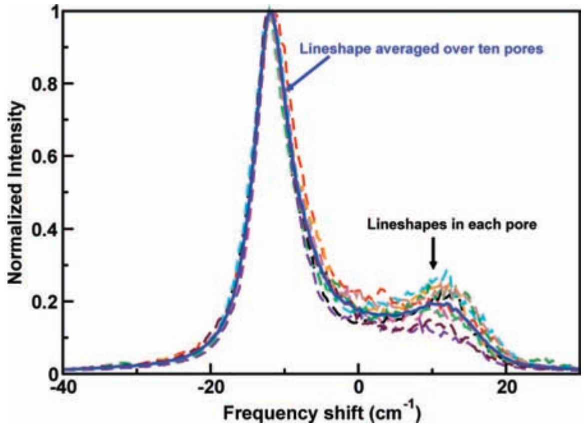

Figure 3. Calcuated spectra for the C$\equiv$N stretch of CH$_3$CN in 10 individual $\approx$2.4 nm diameter silica pores (dashed lines). The averaged line shape (solid blue line) is shown for comparison.

dynamics as well as the effects of the condensed phase liquid structure on the quantum mechanical frequencies may be needed to establish a more quantitative prediction of the infrared line shape.

3. Calculated Infrared Spectra of CH$_3$CN

The simulated infrared spectral line for the ν_2 stretch of bulk CH$_3$CN is shown as a solid black line in Figure 2. The peak shift of 11.4 cm^{-1}, relative to the gas-phase spectrum, is close to the literature infrared peak shift of 12.9 cm^{-1} (obtained after a small correction for Fermi coupling).[30] The calculated fwhm of 4.6 cm^{-1} for bulk CH$_3$CN is in reasonable agreement with a literature fwhm of 5.9 cm^{-1} for a Lorentzian fit[64] assigned to the main ν_2 fundamental in the infrared spectrum.

More important for our purposes is the comparison of our calculated spectral line for bulk CH$_3$CN to that of CH$_3$CN confined to cylindrical silica pores approximately 24 Å in diameter. The most prominent new feature is a shoulder peak on the higher frequency side, similar in location to those observed experimentally.[13,34] The shoulder peak has previously been attributed[13] to hydrogen bonding due to its absence in spectra of acetonitrile confined to hydrophobic silica pores. However, some confusion exists in the literature[13,65] as to whether this shoulder is due to an intrinsic frequency shift upon hydrogen bonding or to a difference in Fermi coupling upon hydrogen bonding, because of the proximity of the shoulder to the nearby ($\nu_1 + \nu_3$) combination band. Our simulations confirm that the shoulder can be explained by an intrinsic frequency shift. As shown by the red trace in Figure 2, the shoulder does not appear in the simulated spectrum unless a correction term is applied to model specific hydrogen bonding effects on the vibrational frequency due to charge transfer (as described in subsection 2.4). This provides direct support for the assignment of the blue-shifted shoulder peak to CH$_3$CN molecules that are hydrogen bonded to silanol groups on the pore wall.

More subtle features of the spectrum also compare well with experiment. The average frequency $\langle\omega\rangle$ is slightly blue shifted relative to the bulk spectrum, consistent with published infrared[34] and isotropic Raman[13] data. The fwhm of the main (red shifted) calculated infrared spectral line for confined CH$_3$CN is 6.5 cm^{-1}, or $\approx$ 40% broader than the fwhm calcuated for bulk CH$_3$CN. This is reasonably similar to the $\approx$40% broadening observed by Nikiel and co-workers for the isotropic Raman line, from a fwhm of $\approx$5 cm^{-1} to $\approx$7 cm^{-1}.[13] The isotropic Raman line shape is another measure of the same vibrational dynamics and differs from the infrared only through the polarizability dependence on the vibrational coordinate; thus it would not be surprising if the infrared spectrum was similarly broadened as our calculations suggest. Other workers have used infrared spectroscopy to study acetonitrile confined to MCM-41 with pore diameters of 3.2 nm.[41] In this study, the ν_2 peak and shoulder were deconvoluted into a sum of three Lorentzians (two for hot bands and one for the main peak) and a Gaussian (for the shoulder). Little to no broadening was reported for the Lorentzian representing the main peak in the confined liquid, relative to the corresponding Lorentzian in the bulk spectrum. Because some broadening upon confinement was thus attributed by those authors to overlap with the shoulder that arises from hydrogen bonding, dynamical effects on the line width were considered to be small. Deconvolution into one Lorentzian (no hot bands) and one Gaussian does not adequately fit our simulated line shape for confined CH$_3$CN because there is a larger separation between the main and shoulder peaks; this separation may be artificially enhanced due to the limitations of our quantum correction.

The calculated spectra for 10 individual model pores are shown in Figure 3 along with the line shape averaged over all 10 pores. While the line width and peak shift of the dominant peak are quite insensitive to the structural heterogeneity of the 10 model silica pores, it is clear that the relative intensity of the shoulder peak varies substantially with the characteristics of individual pores. In fact, the shoulder intensity scales reasonably well with the number of silanol groups in each pore. Interestingly, this contrasts with the case of the cis/trans conformational equilibrium for ethylene glycol, which changes substantially from pore to pore but apparently is not related to the number of silanol groups in each pore.[24] However, it is important to note that our calculations indicate a significant non-Condon effect[51] in which the transition dipole moment for acetonitrile molecules involved in hydrogen bonding with a charge transfer component is ~2 times greater than those which are not. Thus, one cannot use simply the areas under the two peaks to determine the relative number of hydrogen bonded and non-hydrogen bonded CH$_3$CN molecules.

To understand the origin of the observed spectral features, it is necessary to further consider the structure and dynamics of CH$_3$CN confined in silica pores as well as in the bulk liquid. These are examined in the next section.

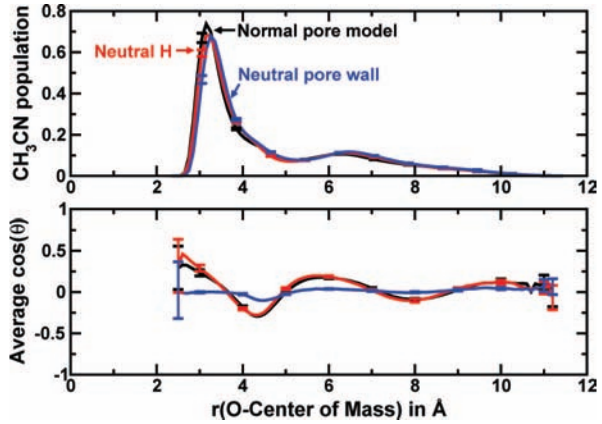

Figure 4. Top: Solvent center-of-mass population. Bottom: Average orientation as a function of r = distance between CH_3CN center-of-mass and the nearest O atom on the pore walls. The angle θ is defined between the molecular axis (from C to N) and the radial vector (from the central pore axis to the CH_3CN center-of-mass). Consequently, $\theta > 0$ where N atoms are oriented toward the surface; $\theta \approx 0$ for molecules oriented parallel to the pore wall; and $\theta < 0$ for N atoms oriented toward the pore interior. Error bars were generated from deviations from the average over 10 pores.

4. Analysis and Discussion

4.1. Liquid Structure. The model silica pores constructed previously[23] and employed in this study were based on a cylindrical shape, but with rough interior surfaces. Because cylindrical symmetry cannot be assumed, a molecule−wall distance coordinate was defined by the distance between the center-of-mass of a given CH_3CN molecule and the nearest O atom on the pore wall. One interesting property of a confined liquid is the population as a function of this molecule−wall distance coordinate, shown in the top panel of Figure 4. Viewed in this coordinate system, the liquid layering is qualitatively similar to that found in previous simulations of liquids confined to smooth-walled spherical and cylindrical pores.[20−22,66,67] Namely, the confined liquid is organized in layers radiating inward from the pore surface.

The bottom panel of Figure 4 depicts the average orientation of CH_3CN molecules as a function of the CH_3CN−wall distance. The angle θ is defined between the molecular axis from C to N and the radial vector from the central pore axis to the CH_3CN center-of-mass, such that $\cos\theta > 0$ for molecules with the N atom oriented outward toward the pore wall. For CH_3CN molecules within ≈3.5 Å of the pore wall, the N atom is oriented preferentially toward the wall, but for molecules between ≈3.5 and 5 Å from the pore wall, the opposite orientational preference prevails. On comparison of the top panel of Figure 4, the molecules ≈3.5−5 Å from the pore wall form a distinct shoulder on the first peak of the radial population. We can interpret the first peak of the radial population as consisting of two orientationally distinct sublayers: in the first sublayer, molecules with center-of-mass distances less than ≈3.5 Å from the pore wall have N atoms tilted generally toward the pore wall, while molecules in the second sublayer have the opposite average orientation. The longer average distance from the wall to the center-of-mass for molecules in the second sublayer may reflect weaker interactions between the relatively nonpolar CH_3 group and the pore wall, given that the Lennard-Jones radius of the CH_3 group is only ~0.2 Å further from the CH_3CN center-of-mass than that of the N atom. The average angle between the radial vector and surface CH_3CN molecules within ≈3.5 Å of the pore wall is ≈60°, indicating that these molecules are not directly perpendicular to the surface. Similarly, the average angle for molecules ≈3.5−5 Å from the wall is ≈120°, indicating that molecules in the second sublayer are generally angled away from the wall and on average are antiparallel to those in the first sublayer.

On the basis of optical Kerr effect data, Fourkas and co-workers have proposed the idea that two antiparallel sublayers exist within the first "layer" of CH_3CN near the pore walls and that more strongly bound molecules have N atoms oriented toward the pore wall.[35−37] Fourkas and co-workers[37] suggested that hydrogen bonding dictates the orientational preferences of the first two sublayers. Clearly, hydrogen bonded CH_3CN molecules must have N atoms oriented toward the pore walls. With a high barrier to rotation attributed to specific hydrogen bonding interactions, the first sublayer could have a very rigid structure enforced by a persistent hydrogen bonded network. The second sublayer could thus be explained in terms of an interdigitated structure similar to that of frozen CH_3CN.

The present simulations indeed confirm that two sublayers with opposite orientational preferences give rise to a peak in radial population near the pore walls and that the molecules nearest the pore walls are preferentially oriented with N atoms facing the pore wall. Insight into the origin of this liquid structure can be gained by considering how the distribution of CH_3CN orientations is affected by hypothetically removing some or all of the charges used to model liquid−wall interactions. The red traces in Figure 4 represent the liquid structure from simulations in which the hydrogen bonding is "turned off". Specifically, the charge on each silanol H atom is absorbed into the charge on the associated silanol O atom, thus removing the charge separation required for hydrogen bonding without significantly affecting other electrostatic interactions. Interestingly, no significant change is seen in the radial population or average orientation as a function of distance. The blue traces in Figure 4 represent the liquid structure from simulations with no partial charges on silica. In this neutral pore model, a similar layered structure emerges in the radial population but the orientational preferences average to zero. Taken together, these comparisons suggest that electrostatic liquid−wall interactions play a key role in determining orientational structure within the confined liquid, but specific hydrogen bonding does not.

Another interesting result is that is the orientational preferences of the surface sublayers are echoed in sublayers further from the wall but are less pronounced. The bottom panel of Figure 4 shows that the liquid between ≈5 and 7 Å from the pore wall is oriented preferentially with N atoms toward the pore wall and that liquid between ≈7 and 9 Å from the pore wall is oriented preferentially in the opposite direction. Together, the two orientationally distinct sublayers in this range from ≈ 5 to 9 Å account for the second peak in the radial population.

While Figure 4 only shows average orientations, Figure 5 shows the distribution of molecular orientations as a function of the center-of-mass distance from pore walls. The corresponding radial populations are overlaid in black to show how angular distributions relate to the layered structure of the confined liquid. Higher contours indicate a higher probability for molecules to have a given orientation at the corresponding distance. Lower probabilities for a given orientation and distance also generally correspond to a barrier in the potential of mean force. The three contour plots (top to bottom) represent simulations with a normal charge distribution, with no charge separation on silanol and hence no hydrogen bonding, and within neutral pores, respectively.

The top panel shows the orientational distribution within the normal charge model, overlaid with the radial population for reference. Two orientationally distinct sublayers are clearly seen

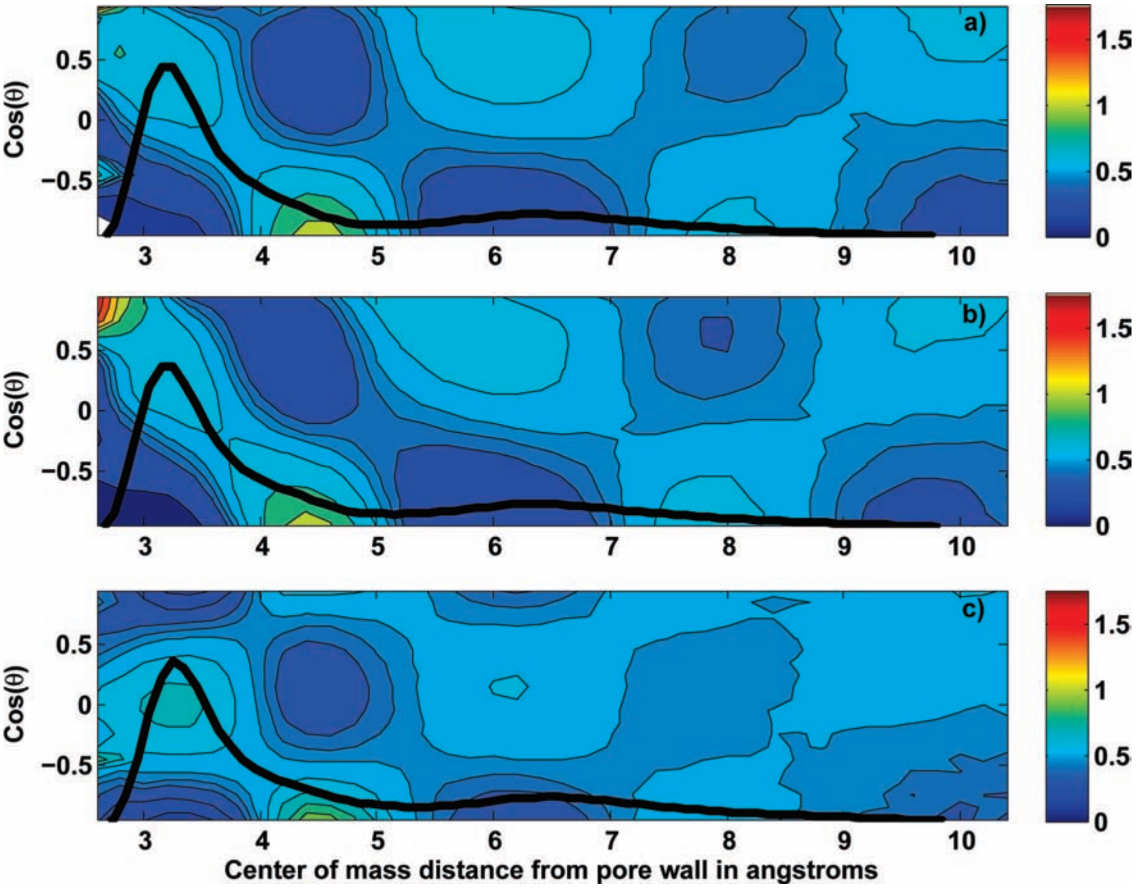

Figure 5. Contour plot of the distribution of CH_3CN orientations as a function of center-of-mass distance from the pore wall for (a) the normal charge model, (b) the hypothetical model with no charge separation on silanol groups, and (c) the hypothetical model with no charges on the silica walls. Overlaid black lines represent the population, also shown in Figure 4. The angle θ is defined as in Figure 4.

to contribute to the first peak in the radial population. In the first sublayer, centered at less than 3 Å from the pore wall and extending to a distance of ≈3.5 Å, CH_3CN shows a strong orientational preference toward the wall as previously discussed. The contours show a wide distribution of angles within the first sublayer but also show that molecules nearest to the surface favor more nearly perpendicular angles. The second sublayer, with the opposing orientational preference, is centered at ≈4.5 Å from the pore wall and covers distances of ≈3.5−5 Å from the pore wall. Again, the contours show a wide distribution of angles, but the molecules at ≈4.5 Å favor a more perpendicular orientation. Similar but weaker orientational preferences are echoed in the two sublayers contributing to the second peak in the radial population.

Small anomalies are perceptible in the orientational distributions for molecules less than ≈2.7 Å from the pore wall. Narrow peaks can be seen at both positive and negative values of cos(θ), in all three panels of Figure 5. Further analysis of simulation data shows that these anomalies can be assigned to molecules that are isolated by more than 5 Å from the nearest neighboring liquid molecule. Apparently, some CH_3CN molecules inserted in the grand canonical Monte Carlo simulations used to fill the pores are trapped in small pockets along the rough silica surface where rotational motion is sterically hindered and their orientations are likely dictated by the specific nature of the trapped sites.

Effects of hydrogen bonding and electrostatic interactions at the pore wall on the liquid structure can be seen by comparing the three panels of Figure 5. The contours in the second panel that result from simulations with no charge separation on the silanol groups are qualitatively similar to those in the first panel. Orientational distributions thus appear to be fairly insensitive to hydrogen bonding interactions, even near the liquid−wall interface. In contrast, the bottom panel of Figure 5 illustrates the dramatic influence of electrostatic interactions with the silica on the orientational distribution of CH_3CN. The confined liquid is still structured in sublayers with distinct orientational preferences, but CH_3CN molecules nearest the surface prefer to lie more parallel to the pore wall in the absence of electrostatic liquid−wall interactions. In the second sublayer, more perpendicular orientations are favored with N atoms oriented both toward and away from the pore wall. This pattern of orientational preferences is echoed in the two sublayers forming the second peak in the radial population. Although electrostatics have a dramatic influence on the orientational distributions, they do not appear to be solely responsible for the propagation of orientational preferences into the interior sublayers.

Similar orientational preferences at the interface were reported by Krilov and Laird for a simulation of a polar liquid near a wall with embedded point charges.[68] In their model system however, liquid layering near the interface propagates through several layers but the accompanying orientational preferences do not.[68] This supports the present conclusion that orientational preferences are governed by the electrostatic field at the interface, but the propagation of these preferences is not. However, packing effects in confined liquids can propagate orientational preferences inward through several layers. Similar orientational distributions have previously been predicted for liquids in nonpolar, smooth-walled pores.[69]

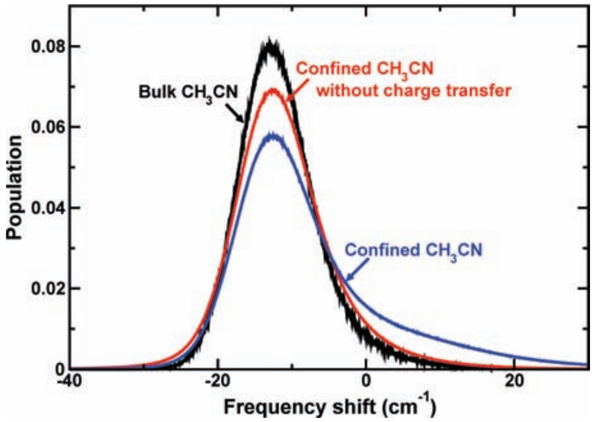

Figure 6. Distribution of calculated C≡N vibrational frequencies for bulk CH_3CN (black line), confined CH_3CN confined (blue line), and CH_3CN without the charge transfer hydrogen bonding correction (red line). All results for confined CH_3CN were averaged over 10 model silica pores.

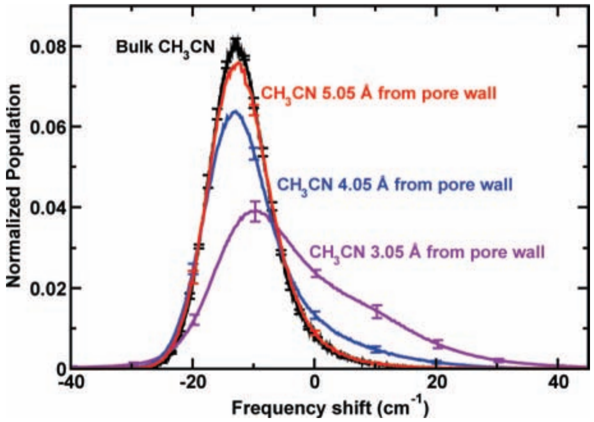

Figure 7. Distribution of calculated frequencies for CH_3CN molecules at specified distances from the pore wall. The frequency distribution calculated for bulk CH_3CN is shown for comparison (black line). Frequency distributions are shown for CH_3CN molecules 3.05 Å (purple line), 4.05 Å (blue line), and 5.05 Å (red line) from the pore wall.

4.2. How Does the Liquid Structure Affect Frequency Distributions? Two factors giving rise to an infrared line shape are the distribution of frequencies and the vibrational dynamics. The distributions of calculated instantaneous vibrational frequencies for bulk (black line) and confined (blue trace) CH_3CN are shown in Figure 6. On comparison of these two, the most obvious difference is the shoulder on the high-frequency side of the distribution for confined CH_3CN. Although not as pronounced as in the infrared line shape, this shoulder must arise from hydrogen bonding. This is clear by comparison to the distribution of frequencies for confined CH_3CN obtained with no correction term for the charge transfer effects of hydrogen bonding on the vibrational frequency, also shown (red line) in Figure 6. Just as in the IR spectra shown in Figure 2, the frequency distribution for confined CH_3CN is very similar to that of the bulk and lacks the characteristic shoulder unless a quantum correction to simulate frequency shifts due to hydrogen bonding is included.

To clarify the relationship between vibrational frequencies and position within the pore, frequency distributions were determined as a function of molecular distance from the pore wall. As shown in the first panel of Figure 7, the frequency distribution of CH_3CN molecules at a very close distance of 3.05 Å from the wall has a broad shoulder due to a substantial population of strongly hydrogen bonded CH_3CN molecules near the surface. Just 1 Å further away at 4.05 Å from the wall, the shoulder is much less noticeable. This remnant of a shoulder at 4.05 Å is due to frequency corrections for weak hydrogen bonding at long range and may not be realistic in a liquid because the correction was parametrized for isolated CH_3CN interacting with a silanol molecule, rather than for liquid CH_3CN in which other molecules may screen the interaction. Nevertheless, CH_3CN molecules 5.05 Å from the pore wall have a frequency distribution very similar to that of the bulk liquid. Such a dramatically short-ranged effect on the frequency distribution explains why the effect of confinement on the infrared line shape depends so strongly on the fraction of liquid molecules in contact with the wall.

Infrared spectra for CH_3CN confined in porous silica have previously been interpreted[34] in terms of a two-state model.[7] In particular, because the shoulder peak is associated with hydrogen bonding at the liquid−wall interface, two "states"—hydrogen bonded and nonbonded CH_3CN—are evident. The present simulations bolster this intepretation by showing that the effect of confinement on the frequency distribution is limited to short-ranged interactions with the pore walls and that molecules closer to the pore interior have a bulklike frequency distribution. Consequently, it is not surprising that the relative intensity of the shoulder peak should scale with the surface area of the confining structure and with the number of silanol groups available for hydrogen bonding. However, care must be taken not to overinterpret the data in terms of a two-state model. The frequency distribution for CH_3CN molecules 3.05 Å from the wall in Figure 7 is clearly bimodal, showing that there is a substantial population of CH_3CN molecules close to the wall that are not hydrogen bonded whose frequency distribution is similar to that of CH_3CN molecules in the pore interior. Although this population of non-hydrogen-bonded surface CH_3CN molecules does not have a distinctive frequency shift like that of hydrogen bonded CH_3CN molecules, their vibrational *dynamics* could be quite different than those of bulk CH_3CN as will be shown in the following section.

4.3. How Do the Dynamics Affect the Spectra? The frequency autocorrelation function, $C_\omega(t)$, defined in eq 9, illustrates the time scale for pure vibrational dephasing and can be related to the liquid dynamics on a molecular level. Thus, $C_\omega(t)$ can serve as a probe of changes in the dynamics of CH_3CN upon confinement that are relevant to the vibrational spectra. Figure 8 shows the calculated normalized frequency autocorrelation functions of CH_3CN in the bulk liquid and confined to the model silica pores. The correlation function for bulk CH_3CN can be fit to a single exponential decay with a time constant of 65 fs. This compares fairly with a measured correlation time of $\approx$100−300 fs based on a line width analysis.[70] For confined CH_3CN, the decay is clearly multiexponential—a sum of three exponentials with time scales of 70 fs, 5 ps, and 134 ps are required to fit $C_\omega(t)$. Although part of the decay occurs on a fast time scale of 70 fs that is similar to that of bulk CH_3CN, a significant component of the decay occurs on a very slow time scale. The short and long time scales are also bridged by an intermediate time scale of $\approx$5 ps.

Figure 8 also shows how hydrogen bonding and electrostatics may affect $C_\omega(t)$ for confined CH_3CN. Specifically, the correlation function obtained without the charge transfer hydrogen bonding correction also has a long time scale decay but with a significantly smaller amplitude than the full result. The long time decay is somewhat slower in the absence of the hydrogen bonding correction. Both of these changes in $C_\omega(t)$ are consistent with the idea that frequencies of hydrogen bonded CH_3CN

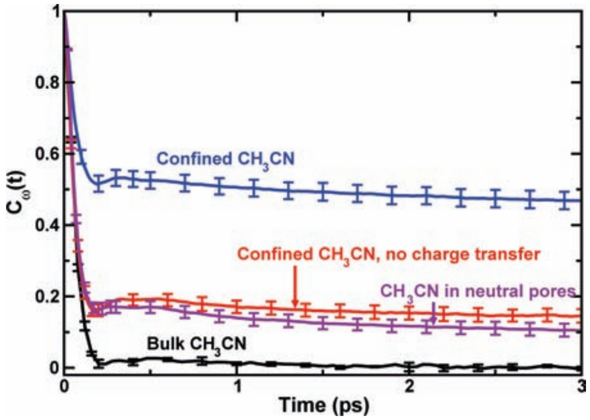

Figure 8. Normalized vibrational autocorrelation functions $C_\omega(t)$ for bulk CH$_3$CN (black line), CH$_3$CN confined in silica pores (blue line), CH$_3$CN in silica pores with no charge transfer hydrogen bonding correction (red line), and CH$_3$CN in silica pores with no charges on silica (purple line). Error bars for confined CH$_3$CN were generated from deviations from the average over 10 pores, while error bars for bulk CH$_3$CN were generated from deviations from the average over four blocks taken from two trajectories.

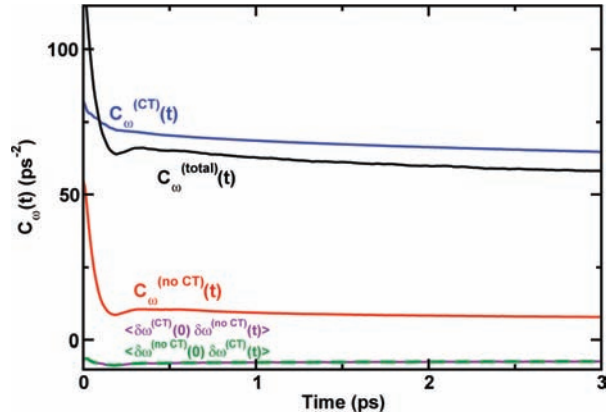

Figure 9. Contributions to the vibrational autocorrelation function, $C_\omega(t)$, associated with the charge transfer hydrogen bonding correction and cross terms for confined CH$_3$CN; see the text.

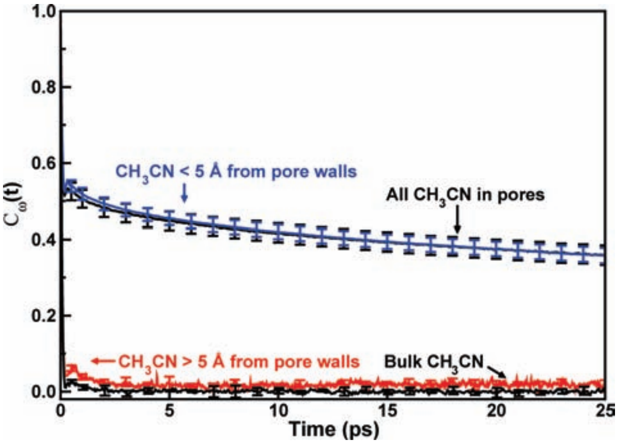

Figure 10. Normalized vibrational autocorrelation functions for CH$_3$CN at r < 5 Å (blue trace) and r > 5 Å (red trace) from the pore walls. Normalized vibrational autocorrelation functions are also given for bulk and confined CH$_3$CN (black dot-dashed and solid traces) for comparison. The decay for molecules toward the pore interior at r > 5 Å (red trace) is similar to that in the bulk. In contrast, the vibrations of molecules near the pore walls decay partially on the same time scale as in the bulk, but part of their decay occurs over a much longer time scale.

molecules are more likely to decay on a long time scale. However, the long time decay is not solely a result of the hydrogen bonding correction. Motions associated with this longer time scale could also be affected by electrostatic interactions between CH$_3$CN and the pore walls. To test this idea, the correlation function obtained in a neutral silica pore is also shown in Figure 8. In this case, the long time component of $C_\omega(t)$ decays somewhat more quickly than under the normal charge scheme in the absence of a hydrogen bonding correction, but at short times the two are the same within error bars. This indicates that the long time decay observed in the simulated correlation functions is due not only to hydrogen bonding-induced frequency shifts and electrostatic interactions but also to slow dynamics associated with, for example, packing of the acetonitrile molecules in the confined environment.

The hydrogen bonding contribution to the simulated $C_\omega(t)$ can also be quantified by considering the unnormalized autocorrelation function $\langle\delta\omega(0)\delta\omega(t)\rangle$. This can be written as a sum of autocorrelation and cross-correlation functions as follows

$$\langle\delta\omega(0)\delta\omega(t)\rangle = \langle\delta\omega^{\mathrm{CT}}(0)\delta\omega^{\mathrm{CT}}(t)\rangle + \langle\delta\omega^{\mathrm{noCT}}(0)\delta\omega^{\mathrm{noCT}}(t)\rangle + \langle\delta\omega^{\mathrm{CT}}(0)\delta\omega^{no\mathrm{CT}}(t)\rangle + \langle\delta\omega^{\mathrm{noCT}}(0)\delta\omega^{\mathrm{CT}}(t)\rangle \quad (19)$$

As can be seen from Figure 9, the cross terms between the hydrogen bonding contribution and the uncorrected frequencies are small compared to the autocorrelation functions of these contributions. It is evident from the $\langle\delta\omega^{\mathrm{CT}}(0)\delta\omega^{\mathrm{CT}}(t)\rangle$ result shown in Figure 9 that the charge transfer hydrogen bonding contribution does not substantially decay on the subpicosecond time scale characteristic of bulk CH$_3$CN. Rather, most of the decay of this contribution occurs on a long time scale on the order of hundreds of picoseconds. The decay of the uncorrected frequency correlation function $\langle\delta\omega^{\mathrm{noCT}}(0)\delta\omega^{\mathrm{noCT}}(t)\rangle$ also has a long time component, but with a much smaller relative amplitude. Because they occur on the same time scale, molecular motions associated with the long time component of the vibrational dephasing of confined CH$_3$CN appear to be strongly correlated with the magnitude of the frequency shift due to hydrogen bonding. The hydrogen bonding correction is an analytical function of distance and angle, so the motion on this time scale could be radial, angular, or some combination of the two.

Because bulklike vibrational dynamics are not recovered even in the neutral pore model (see Figure 8), "pure" confinement effects such as packing of the liquid into layers must also make an important contribution to the motion occurring on a long time scale. Recalling the layered structure of the liquid near the surface as shown in Figures 4 and 5, slower diffusion can be expected due to packing effects within the first two surface sublayers. This is consistent with recent results using the Smoluchowski equation to describe solute diffusion dynamics in nanoconfined liquids, where a similarly long time scale on the order of hundreds of picoseconds was associated with radial solute diffusion away from the walls of a smooth, cylindrical pore filled with CH$_3$CN.[67]

We can investigate the overall effect of the liquid structure on vibrational dynamics by considering separately the liquid molecules that remain within 5 Å of the pore walls and those that remain beyond 5 Å of the pore walls, within the correlated time interval of 25 ps. Figure 10 shows that these two subpopulations of the liquid within the pores differ dramatically in the behavior of $C_\omega(t)$. For CH$_3$CN within the interior of the

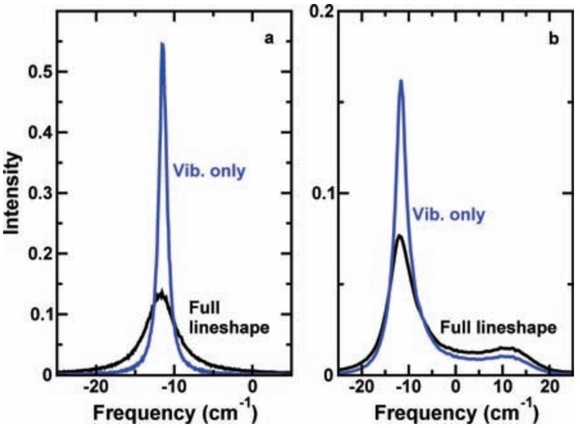

Figure 11. Simulated line shapes for the C≡N stretch of (a) bulk and (b) confined CH_3CN. Line shapes generated using eq 6 (black lines) are compared with line shapes neglecting reorientational correlations (blue lines).

pores, the correlation function is nearly indistinguishable from that of bulk CH_3CN. The slow component of $C_\omega(t)$ can thus be attributed solely to CH_3CN in the surface sublayers. It is important to note that most of the confined CH_3CN (~68%) is located in the surface sublayers within 5 Å of the pore walls, as is evident from the radial populations in Figure 4.[71] Recalling, as shown in Figure 6, that most of the CH_3CN near the surface is *not* hydrogen bonded, the slower dynamics near the surface re-emphasizes the existence of this "silent" third state whose slower dynamics may not be accounted for in a two-state model.

4.4. Reorientational Contributions to the Line Widths. It is useful to consider the consequence of different approximations in calculating the spectrum. One approach, which has been discussed by Lawrence and Skinner,[50] is to neglect the reorientational correlations on the basis that these are sufficiently slow compared to the vibrational correlations. The line shapes for bulk and confined CH_3CN are compared in Figure 11 with the results obtained using this approximation. The approximate line shapes are clearly too narrow in both cases, although the approximation is more severe for bulk CH_3CN than in the pores and more severe for the dominant, red-shifted peak in the pores than for the blue-shifted shoulder peak. For confined CH_3CN, neglect of reorientational correlations would affect the relative height of the main and shoulder peaks. This indicates that the rotational motion of both bulk and confined acetonitrile affect the line shape, though to slightly differing degrees.

To probe this further, the normalized reorientational correlation functions,

$$C_{\mathrm{rot}}(t) = \langle \underline{e}(0) \cdot \underline{e}(t) \rangle \tag{20}$$

where $\underline{e}(t)$ is a unit vector along the acetonitrile molecular axis at time t, have been calculated. The correlation functions for bulk and confined CH_3CN are compared in Figure 12. In addition, fits to the correlation functions are also shown (though they are obscured by the functions themselves). The reorientational correlation function for bulk CH_3CN can be fit to a single exponential decay with a time scale of 2.9 ps, approximately an order of magnitude slower than the ~65 fs decay found for the frequency autocorrelation function shown in Figure 8. This decay time compares reasonably with literature values of 1.1 ps (Raman),[13] 1.7 ps (IR),[41] and 1.4 ps (quasi-elastic neutron scattering).[34] Furthermore, extracting a reorientational time from our calculated line shape ($\tau_{\mathrm{rot}} = (2\pi c \nu_{1/2})^{-1}$) yields a quite similar time scale of 2.4 ps. This suggests that obtaining rotational time scales from line widths is justified for bulk CH_3CN.

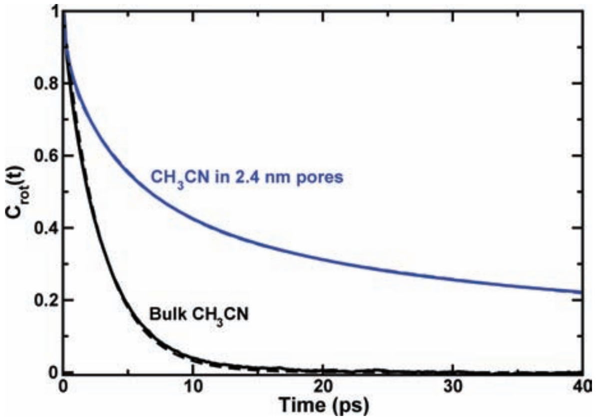

Figure 12. Rotational correlation functions, $C_{\mathrm{rot}}(t)$ (eq 20), for bulk (black line) and confined acetonitrile (blue line) are shown. Fits to each (see the text) are shown as dashed lines of the same color.

However, the situation is more complicated for acetonitrile in silica pores. The rotational correlation function for confined CH_3CN is well fit by a sum of three exponentials, with time scales of 0.5, 5.6, and 63 ps. As noted above, the vibrational correlation function can also be fit to a sum of three exponentials with time scales of 70 fs, 5 ps, and 134 ps. The multiexponential decay of $C_\omega(t)$ and $C_{\mathrm{rot}}(t)$ for the confined liquid is not evident from a standard line shape analysis that assumes a single exponential decay. For example, Tanaka and co-workers determined a correlation time of 1.6−1.7 ps for acetonitrile confined to MCM-41 with 3.2 nm pores based on the deconvoluted infrared line width.[41] This time does not differ substantially from that of bulk CH_3CN. On the other hand, the same procedure applied to our calculated spectrum yields a rotational time based on the line width of ~1.7 ps. This is reasonably similar to the 2.4 ps found for bulk CH_3CN noted above. However, clearly the correlation functions are qualitatively different and such an analysis does not provide an accurate picture of the complex, multiexponential decay on widely varying time scales that is found in the reorientational correlation function. On the other hand, the multiple timescales *are* revealed in optical Kerr effect spectroscopy, where for 2.4 nm diameter hydrophilic sol−gel pores, Loughnane et al. found three exponential time scales for collective reorientation of roughly 1.5, 4, and 20 ps.[36,72] Hence, it is evident that care must be exercised in applying techniques for extracting time scales for rotational and vibrational motions of confined liquids—even when those approaches work satisfactorily for bulk liquids.

5. Conclusions and Future Directions

The infrared spectra of the ν_2 (C≡N stretching) mode of acetonitrile in the bulk liquid and confined in ~2.4 nm diameter hydrophilic silica pores have been simulated using molecular dynamics. The vibrational frequencies were obtained from both classical forces on the basis of first-order perturbation theory and an electronic structure based correction due to charge transfer hydrogen bonding. The calculated spectra are in qualitative agreement with previous experimental measurements.[13,34,41] The spectral features, and their changes upon nanoscale confinement, can be explained based on the structure and dynamics of confined liquid CH_3CN.

The frequency distribution and pure vibrational dephasing of the C≡N stretching mode are both dramatically affected for molecules in contact with the pore walls. In particular, a shoulder

TABLE 2: Fit Parameters for the Hydrogen Bonding Quantum Correction

parameter, X	a_X (cm^{-1})	η_X (Å^{-1})	b_X (cm^{-1})	ξ_X (Å^{-1})	Δ (Å)
A	−464.253	6.26537	−17.7868	0.409428	
α	0.0218571	0.107145	0.0764316	5.10895	0.270092
B	12.2199	1.62874	12.6579	0.531653	
C	0.67558	3.94478			
β	0.0298812	0.62			
D	−0.0263467	0.496322			

arises on the blue-shifted side of the IR spectrum that is directly attributable to hydrogen bonding with surface silanols. The electronic structure parametrized description of hydrogen bonding induced frequency shifts is required to correctly represent these blue shifts. The dominant peak is red shifted relative to the gas phase and is the only peak appearing in the bulk liquid spectrum. In the silica pore this peak is essentially unchanged in position and somewhat broadened (by ~40%). To model the heterogeneity present in porous silica, 10 pore models with the same nominal radius were examined. The dominant spectral peak is insensitive to this heterogeneity, while the blue-shifted shoulder due to hydrogen bonding increases in intensity roughly with the number of surface silanol groups.

The present simulations provide a molecular-level view of the dynamics and intermolecular interactions within the surface CH_3CN sublayers. Radial and orientational population data support the existence of a "surface layer" of CH_3CN near the wall that consists of two sublayers with opposing orientational preferences. Molecules forming the sublayer nearest the wall tend to maximize electrostatic attractions, with their nitrile ends oriented preferentially toward the pore wall. Molecules in the second sublayer orient preferentially in the opposite direction, likely in response to the local electrostatic effect from the first sublayer. Simulation data support a significant barrier to rotation in both surface sublayers, as well as very slow radial diffusion (on the order of hundreds of picoseconds) out of the surface sublayers. These findings are reminiscent of the structural model proposed by Fourkas and co-workers on the basis of optical Kerr effect experiments.[35−37] Mechanistically, simulation results diverge from this model in three ways. First, the orientational preferences near the surface do not depend on hydrogen bonding but are a direct result of electrostatic interactions with the confining silica structure. Second, molecules in the sublayer nearest the surface are not necessarily strictly perpendicular to the surface and are not rigidly bound to specific sites on the wall. As a corollary, the second sublayer forms because of the electrostatic field of the first sublayer rather than falling into a rigid lattice structure. Third, packing effects due to confinement appear to propagate orientational preferences from the surface sublayers into the pore interior.

Thus, the structure of the confined CH_3CN is such that molecules near the rough pore walls experience a range of environments and not all are hydrogen bonded to surface silanol groups. Although CH_3CN molecules that are not hydrogen bonded have a frequency distribution similar to the bulklike distribution for CH_3CN molecules in the pore interior, they have quite different dynamics. For example, a component of their vibrational autocorrelation function decays over a long time scale (>100 ps). This indicates that a two-state model based on the idea of a surface layer with perturbed properties and an interior layer with bulklike properties is not a correct molecular-level description of confined CH_3CN; the reality is somewhat more complex. Moreover, these slower dynamics as probed by the frequency and reorientational correlation functions—which change from single exponential in the bulk liquid to triexponential in the confined liquid—have not been readily apparent from line shape analyses in previous infrared and Raman investigations because a single-exponential time correlation function is often implicitly assumed.

A number of interesting issues remain to be investigated with respect to spectra of nanoconfined liquids. It is likely that a more accurate description of charge transfer and polarization effects associated with hydrogen bonding with the surface silanol groups could be developed. In particular, it would be preferable to include effects on the interactions governing the dynamics as well as the frequency shifts. Also, since localized hydrogen bonding interactions have such a profound effect on the infrared spectrum, there should be an even more noticeable effect on the line shape for some solutes. Specifically, solutes that engage in hydrogen bonding with surface silanol groups could show a dramatic change in their vibrational spectrum when near the pore wall. Conversely, solutes that avoid the pore wall may have line shapes that are more similar to those in bulk solution. Thus, it may be possible to obtain some information about the time a solute spends near the wall from the observable spectral line. Simulations of the dynamics and vibrational spectra of dissolved solutes in liquids confined to silica pores are currently underway in our laboratory.

Acknowledgment. The authors thank Dr. Tolga S. Gulmen for useful discussions. This work was supported by the National Science Foundation (Grant CHE-0518290).

References and Notes

(1) De Vos, D. E.; Dams, M.; Sels, B. F.; Jacobs, P. A. *Chem. Rev.* **2002**, *102*, 3615–3640.

(2) Fierro-Gonzalez, J. C.; Kuba, S.; Hao, Y.; Gates, B. C. *J. Phys. Chem. B* **2006**, *110*, 13326–13351.

(3) Czeslik, C.; Kim, Y. J.; Jonas, J. *J. Phys. IV* **2000**, *10Pr7*, 103–106.

(4) Lee, Y. T.; Wallen, S. L.; Jonas, J. *J. Phys. Chem.* **1992**, *96*, 7161–7164.

(5) Tominaga, K.; Okuno, H.; Maekawa, H.; Tomonaga, T.; Loughnane, B. J.; Scodinu, A.; Fourkas, J. T. In *Liquid Dynamics: Experiment, Simulation, And Theory*; ACS Symposium Series 820; American Chemical Society: Washington, DC, 2002; pp 160−168.

(6) Tan, H.-S.; Piletic, I. R.; Riter, R. E.; Levinger, N. E.; Fayer, M. D. *Phys. Rev. Lett.* **2005**, *94*, 057405.

(7) Piletic, I. R.; Moilanen, D. E.; Spry, D. B.; Levinger, N. E.; Fayer, M. D. *J. Phys. Chem. A* **2006**, *110*, 4985–4999.

(8) Moilanen, D. E.; Levinger, N. E.; Spry, D. B.; Fayer, M. D. *J. Am. Chem. Soc.* **2007**, *129*, 14311–14318.

(9) Zhong, Q.; Steinhurst, D. A.; Carpenter, E. E.; Owrutsky, J. C. *Langmuir* **2002**, *18*, 7401–7408.

(10) Zhong, Q.; Baronavski, A. P.; Owrutsky, J. C. *J. Chem. Phys.* **2003**, *118*, 7074–7080.

(11) Sando, G. M.; Dahl, K.; Zhong, Q.; Owrutsky, J. C. *J. Phys. Chem. A* **2005**, *109*, 5788–5792.

(12) Venables, D. S.; Huang, K.; Schmuttenmaer, C. A. *J. Phys. Chem. B* **2001**, *105*, 9132–9138.

(13) Nikiel, L.; Hopkins, B.; Zerda, T. W. *J. Phys. Chem.* **1990**, *94*, 7458–7464.

(14) Crupi, V.; Majolino, D.; Migliardo, P.; Venuti, V. *J. Phys. Chem. A* **2000**, *104*, 11000–11012.

(15) Hoang, G. C. *J. Korean Phys. Soc.* **2002**, *40*, 224–231.

(16) Kalampounias, A. G.; Kirillov, S. A.; Steffen, W.; Yannopoulos, S. N. *J. Mol. Struct.* **2003**, *651−653*, 475–483.

(17) Kalampounias, A. G.; Yannopoulos, S. N.; Steffen, W.; Kirillova, L. I.; Kirillov, S. A. *J. Chem. Phys.* **2003**, *118*, 8340–8349.

(18) Onori, G.; Santucci, A. *J. Phys. Chem.* **1993**, *97*, 5430–5434.

(19) Rosenfeld, D. E.; Schmuttenmaer, C. A. *J. Phys. Chem. B* **2006**, *110*, 14304–14312.

(20) Thompson, W. H. *J. Chem. Phys.* **2002**, *117*, 6618–6628.

(21) Gomez, J. A.; Thompson, W. H. *J. Phys. Chem. B* **2004**, *108*, 20144–20154.

(22) Mitchell-Koch, K. R.; Thompson, W. H. *J. Phys. Chem. B* **2008**, *112*, 7448–7459.

(23) Gulmen, T. S.; Thompson, W. H. In *Dynamics in Small Confining Systems VIII (Mater. Res. Soc. Symp. Proc.)*; Fourkas, J. T., Levitz, P., Overney, R., Urbakh, M., Eds.; Materials Research Society: Warrendale, PA, 2006; Vol. 899E, p 0899-N06-05.1-10.

(24) Gulmen, T. S.; Thompson, W. H. *Langmuir* **2006**, *22*, 10919–10923.

(25) Gulmen, T. S.; Thompson, W. H. *Langmuir* **2008**, . submitted.

(26) Hench, L. L.; Vasconcelos, W. *Annu. Rev. Mater. Sci.* **1990**, *20*, 269–298.

(27) Luo, R.-S.; Jonas, J. *J. Raman Spectrosc.* **2001**, *32*, 975–978.

(28) Duncan, J. L.; McKean, D. C.; Tullini, F.; Nivellini, G. D.; Perez Peña, J. *J. Mol. Spectrosc.* **1978**, *69*, 123–140.

(29) Loewenschuss, A.; Yellen, N. *Spectrochim. Acta* **1975**, *31A*, 207–212.

(30) Reimers, J. R.; Hall, L. E. *J. Am. Chem. Soc.* **1999**, *121*, 3730–3744.

(31) Fawcett, W. R.; Liu, G.; Kessler, T. E. *J. Phys. Chem.* **1993**, *97*, 9293–9298.

(32) Ben-Amotz, D.; Lee, M.-R.; Cho, S. Y.; List, D. J. *J. Chem. Phys.* **1992**, *96*, 8781–8792.

(33) Nyquist, R. A. *Appl. Spectrosc.* **1990**, *44*, 1405–1407.

(34) Kittaka, S.; Iwashita, T.; Serizawa, A.; Kranishi, M.; Takahara, S.; Kuroda, Y.; Mori, T.; Yamaguchi, T. *J. Phys. Chem. B* **2005**, *109*, 23162–23169.

(35) Loughnane, B. J.; Farrer, R. A.; Fourkas, J. T. *J. Phys. Chem. B* **1998**, *102*, 5409–5412.

(36) Loughnane, B. J.; Farrer, R. A.; Scodinu, A.; Fourkas, J. T. *J. Chem. Phys.* **1999**, *111*, 5116–5123.

(37) Farrer, R. A.; Fourkas, J. T. *Acc. Chem. Res.* **2003**, *36*, 605–612.

(38) Kubo, R.; Toda, M.; Hashitsume, N. *Statistical Physics*, Vol. 2; Springer-Verlag: Berlin, 1985.

(39) Davis, H. T. *Statistical Mechanics of Phases, Interfaces, and Thin Films*; VCH Publishing: New York, 1995.

(40) Gomez, J. A.; Tucker, A. K.; Shepherd, T. D.; Thompson, W. H. *J. Phys. Chem. B* **2005**, *109*, 17479–17487.

(41) Tanaka, H.; Iiyama, T.; Uekawa, N.; Suzuki, T.; Matsumoto, A.; Grün, M.; Unger, K. K.; Kaneko, K. *Chem. Phys. Lett.* **1998**, *293*, 541–546.

(42) The DL_POLY Molecular Simulation Package. http://www.ccp5.ac.uk/DL_POLY.

(43) Gee, P. J.; van Gunsteren, W. F. *Mol. Phys.* **2006**, *104*, 477–483.

(44) Oxtoby, D. W. *Adv. Chem. Phys.* **1981**, *47*, 487–519.

(45) Oxtoby, D. W. *J. Chem. Phys.* **1979**, *70*, 2605–2610.

(46) Rey, R.; Hynes, J. T. *J. Chem. Phys.* **1998**, *108*, 142–153.

(47) Oxtoby, D. W.; Levesque, D.; Weis, J.-J. *J. Chem. Phys.* **1978**, *68*, 5528–5533.

(48) Carbonniere, P.; Bégué, D.; Pouchan, C. *Chem. Phys. Lett.* **2004**, *393*, 92–97.

(49) Alía, J. M.; Edwards, H. G. M. *J. Phys. Chem. A* **2005**, *109*, 7977–7987.

(50) Lawrence, C. P.; Skinner, J. L. *J. Chem. Phys.* **2002**, *117*, 8847–8854.

(51) Schmidt, J. R.; Corcelli, S. A.; Skinner, J. L. *J. Chem. Phys.* **2005**, *123*, 044513.

(52) Deàk, J. C.; Iwaki, L. K.; Dlott, D. D. *J. Phys. Chem. A* **1998**, *102*, 8193–8201.

(53) Oxtoby, D. W. *Adv. Chem. Phys.* **1979**, *40*, 1–48.

(54) Cohen, A. J.; Handy, N. C. *Mol. Phys.* **2001**, *99*, 607–615.

(55) Krishnan, R.; Binkley, J. S.; Seeger, R.; Pople, J. A. *J. Chem. Phys.* **1980**, *72*, 650–654.

(56) Clark, T.; Chandrasekhar, J.; Spitznagel, G. W.; Schleyer, P. V. R. *J. Comput. Chem.* **1983**, *4*, 294–301.

(57) Frisch, M. J.; Pople, J. A.; Binkley, J. S. *J. Chem. Phys.* **1984**, *80* (7), 3265–3269.

(58) Frisch, M. J. ; Trucks, G. W.; Schlegel, H. B.; Scuseria, G. E.; Robb, M. A.; Cheeseman, J. R.; Montgomery, Jr., J. A.; Vreven, T.; Kudin, K. N.; Burant, J. C.; Millam, J. M.; Iyengar, S. S.; Tomasi, J.; Barone, V.; Mennucci, B.; Cossi, M.; Scalmani, G.; Rega, N.; Petersson, G. A.; Nakatsuji, H.; Hada, M.; Ehara, M.; Toyota, K.; Fukuda, R.; Hasegawa, J.; Ishida, M.; Nakajima, T.; Honda, Y.; Kitao, O.; Nakai, H.; Klene, M.; Li, X.; Knox, J. E.; Hratchian, H. P.; Cross, J. B.; Bakken, V.; Adamo, C.; Jaramillo, J.; Gomperts, R.; Stratmann, R. E.; Yazyev, O.; Austin, A. J.; Cammi, R.; Pomelli, C.; Ochterski, J. W.; Ayala, P. Y.; Morokuma, K.; Voth, G. A.; Salvador, P.; Dannenberg, J. J.; Zakrzewski, V. G.; Dapprich, S.; Daniels, A. D.; Strain, M. C.; Farkas, O.; Malick, D. K.; Rabuck, A. D.; Raghavachari, K.; Foresman, J. B.; Ortiz, J. V.; Cui, Q.; Baboul, A. G.; Clifford, S.; Cioslowski, J.; Stefanov, B. B.; Liu, G.; Liashenko, A.; Piskorz, P.; Komaromi, I.; Martin, R. L.; Fox, D. J.; Keith, T.; Al-Laham, M. A.; Peng, C. Y.; Nanayakkara, A.; Challacombe, M.; Gill, P. M. W.; Johnson, B.; Chen, W.; Wong, M. W.; Gonzalez, C.; Pople, J. A. *Gaussian 03, Revision D.01*; Gaussian, Inc.: Wallingford, CT, 2004.

(59) Glendening, E. D.; Badenhoop, J. K.; Reed, A. E.; Carpenter, J. E.; Bohmann, J. A.; Morales, C. M.; Weinhold, F. A. *NBO 5.0*; Theoretical Chemistry Institute, University of Wisconsin: Madison, WI, 2001.

(60) Light, J. C.; Hamilton, I. P.; Lill, J. V. *J. Chem. Phys.* **1985**, *82*, 1400–1409.

(61) Colbert, D. T.; Miller, W. H. *J. Chem. Phys.* **1992**, *96*, 1982–1991.

(62) Dickinson, A. S.; Certain, P. R. *J. Chem. Phys.* **1968**, *49*, 4209–4211.

(63) Meyer, R. *J. Chem. Phys.* **1970**, *52*, 2053–2059.

(64) Hashimoto, S.; Ohba, T.; Ikawa, S. *Chem. Phys.* **1989**, *138*, 63–69.

(65) Busca, G. *Phys. Chem. Chem. Phys.* **1999**, *1*, 723–736.

(66) Thompson, W. H. *J. Chem. Phys.* **2004**, *120*, 8125–8133.

(67) Feng, X.; Thompson, W. H. *J. Phys. Chem. C* **2007**, *111*, 18060–18072.

(68) Krilov, G.; Laird, B. B. *Mol. Phys.* **2000**, *98*, 651–656.

(69) Mitchell-Koch, K. R.; Thompson, W. H. *J. Phys. Chem. C* **2007**, *111*, 11991–12001.

(70) Morresi, A.; Sassi, P.; Paolantoni, M.; Santini, S.; Cataliotti, R. S. *Chem. Phys.* **2000**, *254*, 337–347.

(71) It should be noted that the large number of molecules within 5 Å of the pore surface is due primarily to two factors: the space available (which increases as $2\pi r$ moving away from the pore axis) and attractive interactions with the surface. This number, however, and the populations plotted in Figure 4 (the radial density is not shown) should not be interpreted to mean that the pore interior is vacated. On the contrary, it is similar in density to the bulk liquid.

(72) The optical Kerr effect measurements measure collective orientational reorientation as opposed to our calculations based on individual molecules. Moreover, they are related to $C_2(t) = \langle P_2[\underline{e}(0)\cdot\underline{e}(t)]\rangle$ rather than the $C_{\mathrm{rot}}(t)$ in eq 13 which is presented in Figure 12. Our simulations also give a triexponential decay for $C_2(t)$ with time constants of $\sim$0.3, 3.3, and 52 ps.

JP8072969